High power radiation from ionization fronts in a static electric field in a waveguide

J. R. Hoffman,[a] P. Muggli, R. Liou,[b] M. Gundersen, J. Yampolsky, and T. Katsouleas
University of Southern California, Los Angeles, California 90089

C. Joshi and W. B. Mori
University of California, Los Angeles, California 90089

(Received 27 March 2000; accepted for publication 12 April 2001)

The radiation produced when a relativistically moving plasma/gas boundary (i.e., an ionization front) passes between alternatively biased capacitor electrodes is studied. Results of an experiment based on a design which incorporates the capacitor electrodes into an X band waveguide are presented. The waveguided design effectively couples nearly three orders of magnitude more power into the output than the previously unguided designs. Linear theory is extended to include the depletion of the laser energy as it propagates through the ionizable gas (i.e., laser depletion), and the effect of finite output pulse duration. © *2001 American Institute of Physics.*
[DOI: 10.1063/1.1377608]

I. INTRODUCTION

High power tunable sources of short-pulsed radiation have many applications ranging from advanced ground penetrating radar[1] to characterization of layered dielectrics[2] and plasma reflectometry.[3] Recent work on a technique for generating short (subnanosecond) pulse radiation via ionization fronts moving through a static electric field has yielded tunable radiation pulses in the 6–90 GHz frequency regime.[4,5] These devices convert a static electric field from an alternating capacitor array into radiation when a laser is used to switch the medium between the plates from an insulating gas to a conducting plasma. These so-called dc to ac radiation converters, or DARC sources, provide tunability via changing the gas pressure and/or capacitor spacing, and coherence through the speed of the laser-created ionization front.

The power coupled out of these devices has been fairly modest, typically less than 100 mW per pulse. The limitation on the output power is attributed primarily to two factors: large insertion losses, typically on the order of 30–40 dB, and high voltage breakdown of the gas which places an upper limit on the size of the initial static electric field. In this article, we present results of an experiment on a DARC source structure that overcomes these limitations by incorporating a waveguide into the DARC source design, and by using a high voltage, short pulsewidth, low noise pulser to increase the applied static field. The combined effect of these features is to raise the power coupled out of the device by three orders of magnitude. The results also suggest strategies for achieving higher powers in future DARC devices.

The organization of this article is as follows: in the next section, the theory behind the DARC source is briefly explained, followed by a discussion of a source which is called the pin structure. Section III details the experimental setup used to measure and excite the DARC signal. The experimental results are presented in Sec. IV, the results and some theoretical extensions are discussed in Sec. V, and conclusions and prospects for scaling to even higher powers are described in Sec. VI.

II. THEORY

The mechanism of the dc to ac radiation conversion using ionization fronts is illustrated in Fig. 1. A laser pulse, moving from right to left through an ionizable gas filled region located between alternatively biased electrodes, ionizes the gas as it propagates through, leaving a stationary plasma in its wake. The moving boundary separating the plasma and the gas is called a moving ''ionization front.'' This front shorts the field between the capacitor plates, creating a sequence of dipole-like radiation sources, precisely phased by the group velocity, v_f, of the ionizing laser in the working gas. If the spatial profile of the moving ionization front is ''sharp'' compared with the spacing between pairs of capacitor plates, d, the frequency and the amplitude of the expected output signal can be determined from the boundary conditions of an electrostatic wave of wave number k_0 ''incident'' upon a moving ionization front.[6] Continuity of phase determines the frequency and wave numbers of the four transmitted waves (one electromagnetic at ω_t, one magnetostatic at $\omega_{fs}=0$, and two plasma body modes at $\pm\omega_p$) and the one reflected wave at ω_r. The continuity conditions on the electric and magnetic fields, as well as the currents, determine the relative amplitudes of all of the waves. The expression for the frequency of the transmitted electromagnetic wave is derived in the Appendix for the special case of the volume being bounded by conducting walls forming a waveguide[7] and is equal to

$$\omega_t=[1-\gamma^2\beta^2(-1+\sqrt{1+\kappa_p^2})]k_0\beta_c, \tag{1}$$

where

[a]Electronic mail: jhoffman@physics.usc.edu
[b]Present address: Hughes Aircraft Corporation, Torrance, CA.

 © 2001 American Institute of Physics

Downloaded 14 Aug 2009 to 128.97.48.171. Redistribution subject to AIP license or copyright; see http://jap.aip.org/jap/copyright.jsp

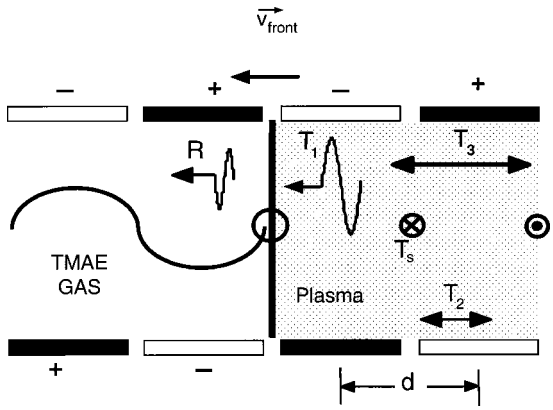

FIG. 1. Schematic of the dc to ac radiation converter. A laser pulse propagates from right to left in an ionizable gas filled region between alternatively biased capacitor electrodes leaving behind a plasma. The moving boundary between the plasma and the gas is called an ionization front. The spacing between the electrodes creating the electrostatic field is characterized by the length *d*.

$$\kappa_p = \frac{1}{\gamma^2\beta^2}\left[\beta^2 - \frac{(\omega_p^2+\omega_c^2)}{\omega_0^2}\right],$$

$\omega_p=(4\pi n_e e^2/m_e)^{1/2}$ is the natural electron plasma frequency; n_e is the plasma electron density; e is the electron charge; m_e is the electron mass; $\omega_c=[(l^2\pi^2)/(a^2)+(m^2\pi^2)/(b^2)]^{1/2}$ is the waveguide cutoff frequency assuming ideally conducting walls; l and m are integers; a and b are the transverse dimensions of the waveguide; $\beta=(v_f/c)=[1-(\omega_p^2/\omega_l^2)]^{1/2}$ is the relative speed of the ionization front with respect to the speed of light, c; $\gamma=[1-\beta^2]^{-1/2}=(\omega_l/\omega_p)$ is the Lorentz factor of the moving ionization front; $\omega_l=(2\pi c/\lambda_l)$ is the laser angular frequency; λ_l is the laser wavelength; and $\omega_0=k_0\beta c$ is the pseudofrequency of the incident electrostatic radiation. For the condition of large frequency upshift, i.e., $\gamma k_0\beta c \gg \omega_p$, this expression reduces to the simplified form[8]

$$\omega_t \cong \frac{k_0\beta c}{2} + \frac{\omega_p^2+\omega_c^2}{2k_0\beta c}. \tag{2}$$

A convenient way to visualize the output frequency and wavenumber of the transmitted wave is to plot the dispersion relation for an electromagnetic wave in a plasma, $\omega_t^2=\omega_p^2+\omega_c^2+k_t^2c^2$, and find the intersection of this curve with the light curve passing through zero frequency at wave number k_0.[6] The light curve is given by $k_0v_f=k_tv_f+\omega_t$ and follows simply from continuity of phase $k_0z=k_tz-\omega_t t$ at $z=-v_f t$, the position of the front. The magnetostatic and Langmuir wave frequencies and wave numbers are also indicated in the figure.

Once the output frequency ω_t is known, the expected pulse width of the output signal can be determined by the following simple formula:[5]

$$\tau \cong \frac{2\pi N}{\omega_t}, \tag{3}$$

where N is the number of cycles present in the initial electrostatic field.

The expected output power is proportional to the square of the transmitted electric field and inversely proportional to the pulse width. The magnitude of the transmitted electric field is determined by solving a boundary value problem with five equations and five unknowns. The details of this analysis and the approximate solutions for the coefficients can be found in Ref. 8. It is found that for large frequency upshifts, the transmitted wave amplitude is approximately equal to the incident wave amplitude. Thus, the magnitude of the output power is proportional to the square of the incident (initial) electric field,[5] and inversely proportional to the pulse width of the generated radiation. In terms of the experiment, the initial electric field strength is controlled by the applied voltage since the electrode vertical separation is held fixed. It was found that using shorter pulse width pulsers, the applied voltage could be increased to ±7 kV.

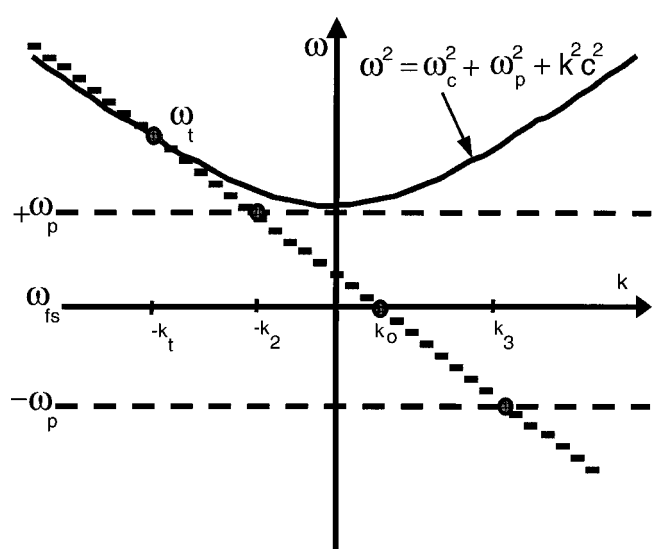

FIG. 2. The intersection between the pin structure dispersion relation, $\omega^2=\omega_c^2+\omega_p^2+k^2c^2$ (solid line), and the light curve, $\omega=(k_0-k)c$ (dashed line), gives the value of the upshifted output frequency, ω_t. The value of the wave numbers for the other modes is also determined by the light curve. The two plasma body modes and the free streaming mode intersection points are shown. The reflected wave frequency and wave number are off scale.

III. DESCRIPTION OF THE EXPERIMENTAL SETUP AND THE PIN STRUCTURE

The experimental setup is shown in Fig. 3. A frequency quadrupled Nd:yttrium–aluminum–garnet (YAG) laser ($\lambda_l=266$ nm) is used to ionize a working gas consisting of TMAE at a pressure of 0.1–100 mT. The plasma density has a quadratic dependency on the laser intensity since TMAE is ionized through a two photon process (ionization potential of 5.36 eV,[9] UV photon energy is 4.6 eV) in this experiment. A solid state high voltage (±15 kV), short pulse width [~80 ns full width at half maximum (FWHM)] pulser is used to alternatively bias an array of electrodes (either pins or plates), creating a static electric field. The generated radiation is detected in the forward direction with microwave diodes using two Tektronix 7912AD oscilloscopes (500 MHz bandwidth) which are triggered by a fast ET2000 photodiode (200 ps rise

Downloaded 14 Aug 2009 to 128.97.48.171. Redistribution subject to AIP license or copyright; see http://jap.aip.org/jap/copyright.jsp

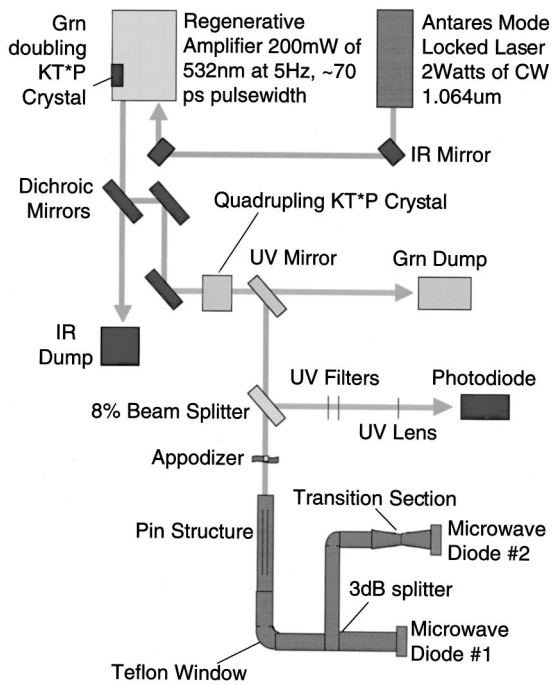

FIG. 3. Schematic plot of the experimental setup. A 1 μm mode locked laser is regeneratively amplified, and doubled twice to produce a laser pulse of light with a wavelength of 266 nm, pulse width of 50 ps, and energy of 30 mJ. The laser then propagates into the pin structure through a UV window and finally terminates in the wall of the waveguide elbow. A Teflon window is used after the elbow to hold the vacuum inside the structure, but allows the generated microwaves to pass through to the microwave diodes.

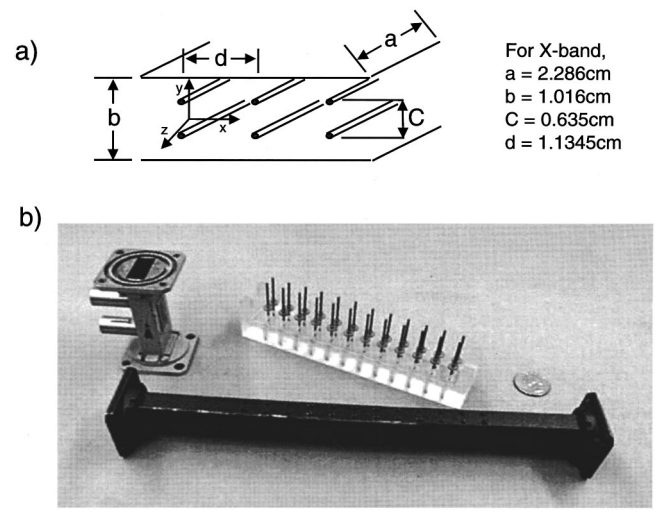

FIG. 4. (a) Diagram of the pin structure geometry. The waveguide cross-sectional dimensions are $a=2.286$ cm and $b=1.016$ cm. The pins are separated vertically by a distance $C=0.635$ cm and spaced longitudinally by a distance $d=1.1345$ cm. (b) Picture of the preassembled pin structure. Also shown is one of the custom made waveguide vacuum sections which allowed the experiment to do without an external vacuum chamber.

time). The UV laser light entering the structure is monitored by using a 8% beamsplitter to send the reflected light into another photodiode (Thorlabs model 20V/579-7227). The applied voltage pulse is monitored using a Tektronix P6105 high voltage probe (75 MHz bandwidth). The UV measuring photodiode and applied voltage signals are recorded using a Tektronix 2440 digital oscilloscope (300 MHz bandwidth). The pressure is measured using a MKS capacitive manometer (1 Torr max), and the applied current is measured using a Rogowski coil (10 V/A into 50 Ω). Both these signals are recorded using a Tektronix 2430A digital oscilloscope (100 MHz bandwidth).

In order to achieve higher output powers than before, the applied voltage, and thus the initial electrostatic field was increased by using a pulser with a faster rise time. It was found that the applied voltage at which breakdown in the DARC source structures occurred varied directly with the applied voltage and inversely with the pulse width of the applied voltage pulse. For example, breakdown in the pin structure (to be described in the next paragraph) would occur at 450 V dc, 6.5 kV with a 300 ns FWHM pulser, and 14 kV with this faster pulser. The high voltage pulser used in this experiment was developed at USC. It can provide pulses of ~80 ns FWHM and up to ± 15 kV into a matched load of 2000 Ω.

Previous DARC sources suffered from poor output power coupling. A common feature of those sources was that all of them were cut transversely to form a capacitor array, thus negating any waveguiding characteristics of the conductor geometries. Therefore, to achieve higher output powers, a restriction on future DARC sources is to not have transverse cuts in the waveguide walls. This restriction and the requirement to insert a capacitor array into the waveguide proved to be relatively simple to overcome. The realization of one concept is shown in Fig. 4. A diagram, and a picture of a waveguide in which stainless steel pins with dielectric collars are inserted into holes drilled into the *E* plane of the waveguide is shown. This structure is referred to as the pin structure. It consists of 12 pairs of pins or rods inserted as shown into a standard *X*-band waveguide. These pins are alternatively biased to produce a static waveform, similar to the one shown in Fig. 1. The transmission properties of the pin structure were tested using an HP 8720 network analyzer (1–20 GHz) and compared to a standard, nonperforated waveguide (Fig. 5). Except for periodic band gaps starting at 14.6 GHz, the transverse properties of the pin structure are indistinguishable from those of a plain waveguide. The periodic stop bands occur when the half-wavelength in the guide matches the pin spacing *d*, or at $\omega_{\text{stop band}}=\sqrt{(m\pi/d)+(l\pi/a)}$ for a TE_{l0} mode. By properly choosing the pin spacing, the periodic stop bands can be designed to fall outside of the nominal frequency range of the waveguide. Another consideration for the choice of the pin spacing is the desired frequency range of interest. If "*d*" is chosen too small, not only will the stop bands be well outside of the waveguide band, but the frequency tunability of the output will become very sensitive to the plasma density (i.e., for small changes in gas pressure and/or laser intensity, large output frequency changes will occur). This can lead to having other modes beside the fundamental $\text{TE}_{1,0}$ being present in the output, which is undesirable for many applications. For the example investigated here, the vertical pin spacing "*C*" was constrained by the waveguide dimensions to be 1.016 cm, and the horizontal pin spacing *d*, was chosen to be 1.1345 cm, making the band gaps fall outside of the *X* band (i.e., the $\text{TE}_{1,0}$ mode, 8.2–

Downloaded 14 Aug 2009 to 128.97.48.171. Redistribution subject to AIP license or copyright; see http://jap.aip.org/jap/copyright.jsp

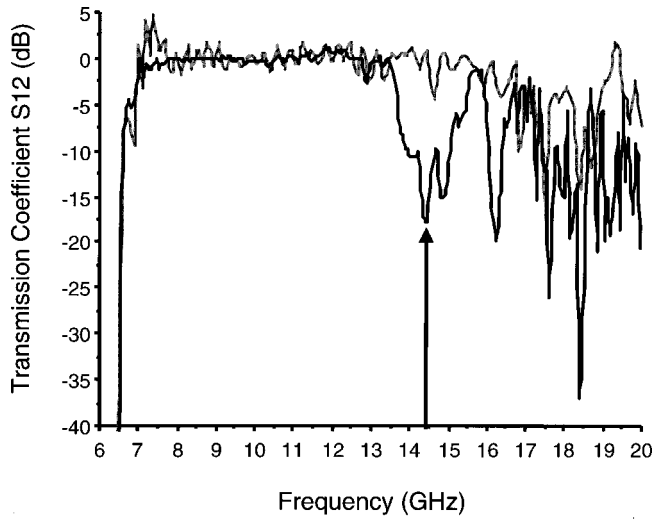

FIG. 5. Cold test of the pin structure with Teflon window (black line) compared to the response of a normal *X*-band waveguide (gray line). The vertical arrow shows the first stop band at 14.6 GHz due to insertion of the pins.

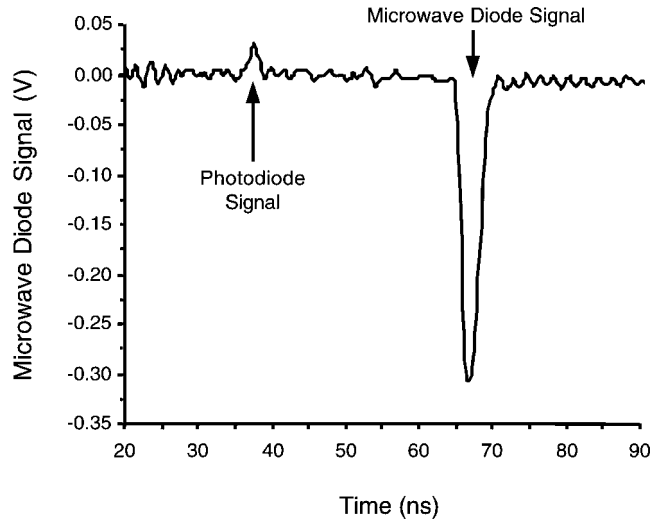

FIG. 6. Oscillogram of the output signal measured by the microwave diode from the pin structure. The first positive peak is the larger pulse signal measured by the fast photodiode. The second negative peak is the signal measured by the microwave diode. There is ~27 ns delay line between the fiducial and the microwave diode signal. The microwave diode signal was attenuated by 5 dB, the applied voltage was ±2 kV, the TMAE pressure was 8 mT, and the pin spacing was 1.1345 cm.

12.4 GHz), with the first stop band at $(m=l=1)$ 14.6 GHz.

The wave number $[k_0=(\pi/d)]$ of the initial electrostatic field could be varied by either alternatively biasing consecutive pin pairs or skipping pin pairs. Skipping pin pairs also has the effect of changing the number of cycles present in the output pulse, and thus reducing the pulsewidth [see Eq. (3)]. In the experiment, the first pair of pins in the direction of laser propagation were left unbiased to avoid a premature breakdown due to photoelectric electrons ejected from the conductors. This means for the case where every pin pair was biased (the $d=1.1345$ cm case), 5.5 cycles are in the pulse, and for the case where every other pin pair was biased (the $d=2.269$ cm case), 3 cycles. Therefore, using Eq. (3) for the $d=1.1345$ cm case and given the desired output frequency range of 8.2–12.4 GHz, the predicted output pulse widths are between 458 and 688 ps. The dependency of the output frequency on the plasma density for these two choices of d is shown in Fig. 13 in the Appendix.

IV. RESULTS

A sample oscillogram of the microwave diode signal as well as a laser pulse fiducial from the fast photodiode is shown in Fig. 6. The instrument limited pulse width, as measured from the figure is approximately 2.9 ns, from which it is inferred that the peak power is actually ~5 times higher than that determined from the calibrated peak microwave diode signal.

The power produced by the pin structure was measured using a calibrated microwave diode and a variable attenuator (0–20 dB). The variable attenuator was used to keep the power reaching the microwave diode below its saturation level of ~100 mW. Figure 7 shows that the power has a quadratic dependency on the applied voltage as predicted by theory.[5]

For this set of data, a power level of ~25 W was achieved with an applied voltage of 3 kV. A factor of 5 attributed to the instrument response time has been included in this plot. The output power of the pin structure seemed to saturate after 3 kV when using the fast pulser, but previous results using a pulser with a slower rise time to apply ~7 kV, showed power levels of up to 100 W.[10] The cause for this apparent saturation is not currently understood, but observation of the inrush currents seems to indicate that the pulser is current limited to 15 amps whereas the slower pulser is not.

The frequency dependence of the signal on plasma density is determined by varying the TMAE gas pressure and using waveguides with different cutoff frequencies. Referring to Fig. 3, one branch of the 3 dB coupler was connected to a normal *X*-band waveguide in order to monitor the shot-

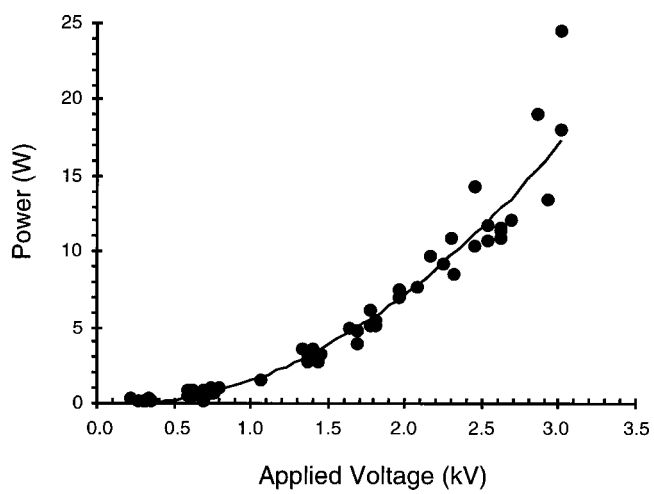

FIG. 7. Power measured as a function of the applied voltage across the pins. A least squared fit (solid line) to the experimental data shows a quadratic dependency of the output power on the applied voltage as predicted by theory. The quadratic coefficient is 2.2117 W/kV^2. A factor of 5 due to pulse width considerations has been included in the plot. The pressure was 14 mT.

Downloaded 14 Aug 2009 to 128.97.48.171. Redistribution subject to AIP license or copyright; see http://jap.aip.org/jap/copyright.jsp

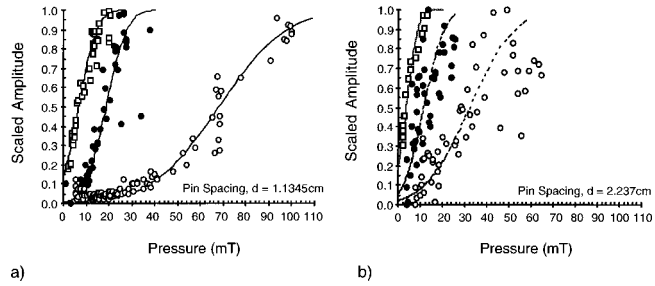

FIG. 8. Plot of the normalized microwave diode signal amplitude vs pressure of TMAE gas. The hollow squares are signal amplitudes measured using an *X*-band transition section. The filled circles are measured with a K_u-band transition section and the open circles are those measured with a *K*-band section. The solid curves are derived from the theoretical model of Sec. V. (a) Pin spacing $d=1.1345$ cm. (b) Pin spacing $d=2.269$ cm. From Sec. V, it is inferred that the half maximum point of each curve corresponds to the waveguide cutoff frequency or signal onset.

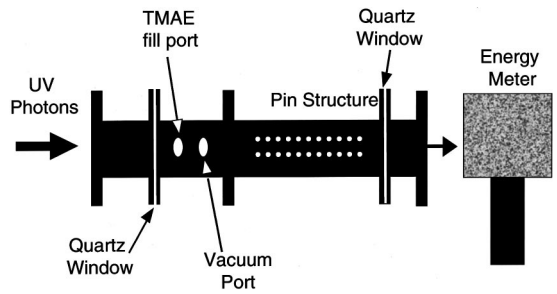

FIG. 10. The depletion of the laser energy was measured by replacing the waveguide elbow and Teflon window after the pin structure with a quartz window. To remove any stray green light, and avoid clipping inside of the pin structure, the UV light was conditioned by passing it through an appodizer and a UV glass (UG5) filter. With no TMAE present in the structure, the total UV energy measured by the radiometer was ~3 mJ. The total length of the ionized volume from the entry window was 30 cm.

to-shot amplitude variations, whereas the other branch was attached to different transition sections.

Figure 8 shows the signals measured with *Ku* (cutoff frequency, $f_c=9.5$ GHz) and *K* ($f_c=14.1$ GHz) band transition sections normalized to the *X*-band reference amplitude on each shot and scaled to unity. Also shown is the *X*-band reference signal normalized to its maximum value. The spread in the data is due to amplitude variations in the laser energy, pressure drift and trigger timing jitter of the pulser. The experimental data was filtered such that for each shot, the applied voltage, the pressure and the UV laser energy varied by less than ±5% from their nominal values. The trend of increasing output frequency with increasing pressure expected from the theory [Eq. (2)] is apparent from the raw data shown in Fig. 8 and the cutoff frequency versus onset pressure curve in Fig. 9. For Figs. 9(a) and 9(b), the onset pressure is taken to be the pressure at which the signal in Figs. 8(a) and 8(b), reach half maximum, respectively. Figure 9 summarizes the dependence of the output signal frequency on pressure, and also shows the dependence of the output frequency on the pin horizontal spacing *d*. The two cases shown are for pin spacings $d=1.1345$ cm and $d=2.269$ cm.

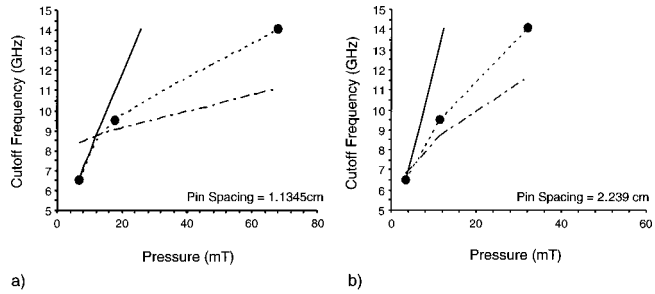

FIG. 9. Plot of the theoretical and experimental onset frequency measurements (half maximum point from Fig. 8) vs pressure for two different pin spacings. The linear theory (solid line) and the experimental data (dashed line, filled circles) diverge at higher pressures. Extending the linear theory with the laser depletion model (dot dashed line, see Sec. V) gives good agreement even at higher pressures. (a) Pin spacing $d=1.1345$ cm. (b) Pin spacing $d=2.269$ cm. Notice that the onset pressure change as a function of pin spacing. If the output signal were due to ω_p radiation, changing the pin spacing should not change the pressure at which the onset frequency is measured.

Quantitative comparison of the experimental results to the theory requires modification of the model of Sec. II to include factors that are present in the experiment such as laser depletion and finite pulse width effects. These will be described in the next section although the results of these modifications are shown in Fig. 9.

V. DISCUSSION

A quantitative comparison between the experimental results and theory requires modification of the simple model to include two important effects present in the experiment: (i) laser depletion (i.e., where the laser loses a significant amount of its energy as it propagates through the ionizable TMAE gas), and (ii) finite pulse width effects (i.e., where the output pulse is not a delta function, but has a finite pulse width).

Laser depletion is assumed to be the reason behind the deviation of the experimental results (dashed line) from the linear model (solid line) shown in Fig. 9. To determine if laser depletion was occurring, the pin structure vacuum configuration was changed such that the transmitted laser energy could be measured as a function of TMAE pressure. The laser depletion experimental setup is shown in Fig. 10. This configuration fixed the length *L* of the ionized volume between the two windows to be 32 cm. The UV energy was measured at the far side of the pin structure through a UV glass filter (UG5). The results of this measurement, presented in Fig. 11(a), show that a decaying exponential (solid line), with an absorption constant $\kappa=0.03$ mT^{-1}, is a good fit to the data. Assuming a spatial exponential decay of the plasma density, and given the length *L* of the volume of ionized gas, the decay constant, $\sigma=(\kappa P_0/L)$, as a function of TMAE pressure P_0 can be determined as shown in Fig. 11(b). The value of σ determined this way compares well with the single ionization decay length of TMAE measured by Shen *et al.*[11] They measured a decay length $(1/\sigma)$ of 35 cm at 60 mT. For the same pressure, the earlier equation yields 16 cm for the two photon process used here. This seems to imply that for our intensity (~2 GW/cm^2), the total photoionization cross section for two photon and single photon ionization are the same. Figure 11(b) depicts the density decay for two

Downloaded 14 Aug 2009 to 128.97.48.171. Redistribution subject to AIP license or copyright; see http://jap.aip.org/jap/copyright.jsp

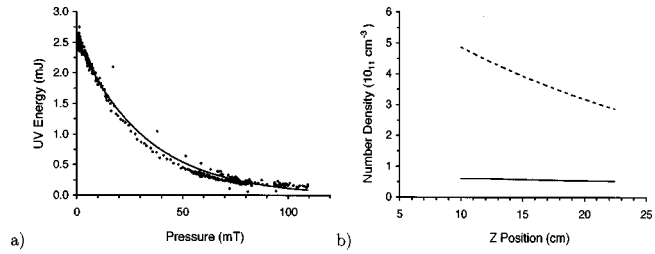

FIG. 11. (a) Measured UV energy passing through the pin structure as a function of TMAE pressure. The decay of the UV is well described by an exponential with a decay constant of 0.03 mJ/mT. (b) The plasma density vs distance along the pin structure assuming an exponential fit for two different pressures: 11.3 mT (dashed line), and 3.5 mT (solid line).

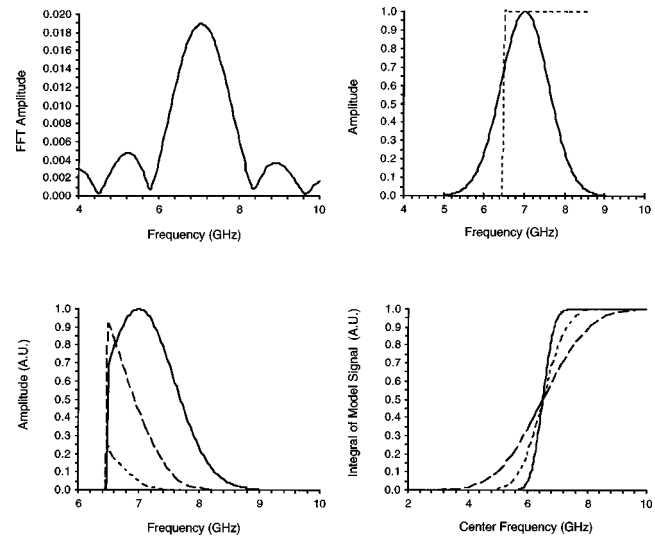

FIG. 12. (a) Fast Fourier transform of a chirped pulse which has an average frequency of 7 GHz, (b) a Gaussian approximation (solid line) for the frequency spectrum of the chirped pulse in part a, and the model representation (dashed line) of the cutoff waveguide behavior in frequency space, and (c) the product, in frequency space, of the cutoff waveguide and three different Gaussian signals of constant pulse width. The areas under each curve is 0.0023, 0.24, and 0.921, respectively, (d) the integral of the square of the frequency domain curves (i.e., the energy) for different pulse widths. The shortest pulse width, 1 ns, has the smallest slope (dashed line), while the longest pulse width, 4 ns, has the steepest slope (solid line). Notice that regardless of the pulse width, all of the curves cross at the same place—the value of the cutoff waveguide and at their half maximum values.

different pressures. At higher pressures, the density gradient is steeper than at lower pressures as would be expected.

A simple model to incorporate the effect of laser depletion into the theory has been developed and is based on the fact that each static field cycle produces one radiation cycle. The frequency of that cycle is assumed to be given by the idealized theory [Eq. (2)] at the plasma density of the location of the pin pair that generated it with an amplitude of unity. The peak value of plasma density, n_e in Fig. 11(b) is obtained from the pressure P, and the linear relationship $n_e = \alpha P/kT$, with $\alpha = 0.0045$. This value of α is a fit to the first (i.e., lowest pressure) data point in Fig. 9 using Eq. (2) (where laser depletion is expected to be the least). The frequency of the pulse train is then estimated by averaging over the half cycles, i.e., $\omega = (\Sigma_{n=1}^{11} E_n^2 \omega_n \delta t_n)/(\Sigma_{n=1}^{11} E_n^2 \delta t_n)$, where δt_n is the duration of a half cycle, (π/ω_n). Figure 9 shows that the modified model (dot-dashed line) is in qualitative agreement with the experimental data (dashed line, large circles) and that the output frequency at a given pressure depends on the pin spacing. This dependency on the pin spacing confirms that the radiation observed is produced through the DARC effect and is not radiation from the plasma at ω_p. We comment that an additional effect on the onset frequency that is not included in the simple model is the effect of the pins on the waveguide dispersion relation. However, this is non-negligible only at the highest frequency in our data set (i.e., 14.1 GHz near the 14.6 GHz stop band), and is not treated here. We expect this to further lower the theory curve in Fig. 9.

The second effect not incorporated in the simple model of Sec. II is that due to the finite pulse length of the produced radiation. The effect of the short pulse length is to broaden the frequency content of the output pulse which would explain the slow rise of the signal strength seen in the cutoff waveguide measurements (Fig. 8). This is quantitatively incorporated into the linear model as follows: the produced output signal is chirped via laser depletion as described in the last paragraph. The exponential decay in the plasma density along the pins always results in the generation of a negatively chirped radiation pulse. A fast Fourier transform of this chirped pulse [Fig. 12(a)] is taken and the resulting frequency spectrum is approximated by a Gaussian fit with either a constant FWHM, or a variable FWHM which depends on the average frequency as predicted by Eq. (3) [Fig. 12(b)]. Modeling the cutoff waveguide as a step function[12] at frequency ω_c [see Fig. 12(b)], the result of the cutoff waveguide measurement is the product of these two functions in frequency space [Fig. 12(c)]. By squaring and integrating this product in frequency space, a value is obtained which is proportional to the energy detected after the cutoff waveguide at each pressure. This "energy" is plotted in Fig. 12(d) as a function of average frequency [which is related to the pressure in the experiment through Eq. (1)] for three different assumed pulse widths and shows that the effect of shorter pulses (i.e., higher output frequency content) is to reduce the slope of the onset plot of the signal. This model further shows that the appropriate value of the pressure at which the output signal is the same as the cutoff waveguide frequency is at the 50% maximum amplitude point on the onset signal plot (Fig. 8). An immediate prediction of this model is that the slope of the onset of the signal should be less using higher frequency cutoff waveguides than lower ones. The results (solid lines) of this model were plotted along with the experimental data in Fig. 8. The agreement between the model and the data is suggestive that short pulse length is the dominant effect in the broadening of the onset of the signal on a particular cutoff waveguide measurement. Unfortunately, a broad frequency spectrum does not necessarily imply a short pulse. The strongest statement that can be made is that the measured frequency spectrum is broad enough to support a short pulse, and the output pulse is faster than the microwave diode can resolve. A comparison between the experimentally inferred and the theoretical pulsewidth calculations from Eq. (3) are presented in Table I. Two different fit methods to the experimental data in Fig. 8 were used. The

Downloaded 14 Aug 2009 to 128.97.48.171. Redistribution subject to AIP license or copyright; see http://jap.aip.org/jap/copyright.jsp

TABLE I. Table of experimentally inferred and theoretically calculated pulse widths for two different pin spacings, *d*. Two different models were used to fit the experimental data: (i) a constant pulse width model in which the pulse width is assumed to be constant as a function of increasing pressure, and (ii) a variable pulse width model in which the pulse width is changing as a function of pressure via the laser depletion model and Eq. (3). Also shown is the percent difference between the experimentally inferred pulse widths and the pulse width predicted by linear theory. The average error is 16%.

	Pin spacing $d=1.1345$ cm			Pin spacing $d=2.269$ cm		
	X band	K_u band	*K* band	*X* band	K_u band	*K* band
Linear theory	846 ps	579 ps	390 ps	462 ps	316 ps	213 ps
Constant pulse width	740 ps	633 ps	210 ps	478 ps	243 ps	219 ps
(% diff)	(12.5%)	(−9.3%)	(46.2%)	(−3.5%)	(23.1%)	(−2.7%)
Variable pulse width	846 ps	661 ps	379 ps	522 ps	225 ps	138 ps
(% diff)	(0.%)	(−14.2%)	(2.8%)	(−13%)	(28.8%)	(35.2%)

first method was to use a constant pulse width and vary the center frequency of the spectrum using the weighted average method described earlier for laser depletion. The second method was to again vary the center frequency, ω_{center}, and vary the pulse width via the following formula: $\tau=(N_0/\omega_{\text{center}})$, where τ is the pulse width, N_0 is a fit parameter. Also shown in Table I are the percent differences between the experimental fits and the theoretical prediction. The experimental values all fall within ±46% of theory, and the average error for the constant pulse width model is ±16.2%, while that for the variable model is ±15.7%.

An estimate of the experimental error for this experiment can be derived as follows: a ±5% in laser intensity produces a ±10% error in the plasma density (two photon ionization process); a ±5% error in the applied voltage measurement produces a ±5% error in signal amplitude,[8] but this implies a ±10% error in the microwave diode output signal (since the diode signal is proportional to the field energy); and a ±5% error in the pressure measurement again implies a ±10% error in the plasma density. Assuming these errors are independent, taking the root sum square of the errors gives an error for the experimental pulse width values of ±17%. The experiment and theory, at least on average, agree fairly well with each other considering the frequency response of the microwave diode at higher frequencies (i.e., outside of the *X* band), and possible multiple waveguide modes being excited which could lead to a modification of the frequency spectra have not been included.

VI. CONCLUSION

The work presented here has demonstrated four aspects of DARC with ionization fronts. First, the viability of a waveguided DARC source for overcoming the insertion losses of the previous geometry's. Second, a 80 ns pulse width voltage pulser was shown to increase the breakdown standoff voltages by a factor of 17 over dc bias, and a factor of 2 over 300 ns pulses. Third, the importance of laser depletion in limiting the frequency upshift conversion was quantified, and fourth, finite pulse width effects are responsible for the rather slow rise in amplitude of the onset of the signal versus pressure/plasma frequency as compared to the waveguide cutoff frequency spectrum (step function profile).

Based on these results, major improvements are possible on two fronts. The use of higher intensity lasers and even shorter pulse width pulsers would significantly increase the frequency and amplitude of the output, respectively. For example, to make a *W*-band (70–110 GHz) structure, the following two options should hold the most promise.

(i) Direct scaling of the dimensions of the *X*-band structure to *W* band would require the pin spacing *d* to be in the range between 1.27 and 2.54 mm, the pin diameter would be reduced to 0.1 mm, the laser pulse width would have to be decreased in order to maintain an ionization front length comparable to the dimensions of the *W* band waveguide, the pins would probably need a dielectric coating to increase the standoff voltage (although, this would require changing the polarity from shot to shot to prevent charge buildup on the dielectric), and the laser would need to be able to produce densities between 6×10^{13} and 1.5×10^{14} cm^{-3}.

(ii) Use the current *X*-band structure, but run it overmoded. This would require densities on the order of 2.9×10^{13} cm^{-3} and to ensure spatial uniformity of the plasma density, the intensity of the laser should be increased by a factor of 3 or more.

ACKNOWLEDGMENTS

This work has been graciously supported by the U.S. D.O.E. under Grant No. DE-FG03-92ER-40745, by the NSF under Grant No. ECS-9632735, and by the AFOSR. J. R. H. would like to thank A. Tan for help with manuscript preparation and everyone in the Neptune lab for their support during those long lonely days of extreme effort with seemingly little payoff.

APPENDIX: DERIVATION OF MODE FREQUENCIES AND WAVE NUMBERS

The various modes excited in and by the moving ionization front can be derived directly from Maxwell's equations, the continuity equation, and the conservation of momentum equation, but if one is interested only in the frequencies and wave numbers of the various modes, a much simpler approach is possible.[13,14] By assuming an infinitely sharp ionization front, the phase of the various modes must match at the moving boundary. In mathematical terms, the phase of the six modes are defined as follows, assuming the ionization front is moving from $+z$ to $-z$ with a velocity v_f, and the incident wave is moving from $-z$ to $+z$:

$$\text{Incident wave:}\quad \phi_i=k_iz-\omega_it, \tag{A1}$$

$$\text{Reflected wave:}\quad \phi_r=-k_rz-\omega_rt, \tag{A2}$$

$$\text{Transmitted wave:}\quad \phi_t=k_tz-\omega_tt, \tag{A3}$$

$$\text{Free streaming mode:}\quad \phi_s=k_sz, \tag{A4}$$

$$\text{Body mode 1:}\quad \phi_1=k_1z-\omega_1t, \tag{A5}$$

$$\text{Body mode 2:}\quad \phi_2=k_2z-\omega_2t. \tag{A6}$$

Downloaded 14 Aug 2009 to 128.97.48.171. Redistribution subject to AIP license or copyright; see http://jap.aip.org/jap/copyright.jsp

Continuity of phase at the moving front boundary, $z=-v_f t$ implies that

$$-(k_i v_f+\omega_i)=(k_r v_f-\omega_r)$$
$$=-(k_t v_f+\omega_t)=-k_s v_f \tag{A7}$$
$$=-(k_1 v_f+\omega_1)=-(k_2 v_f+\omega_2),$$

and with the dispersion relationships

DARC source condition: $\omega_i=0$, (A8)

EM wave in vacuum: $\omega_r=k_r c$, (A9)

EM wave in a plasma filled waveguide: $\omega_t^2=k_t^2c^2+\omega_p^2+\omega_c^2$, (A10)

Langmuir wave: $\omega_1=+\omega_p$, (A11)

Langmuir wave: $\omega_2=-\omega_p$. (A12)

The dispersion relations and the continuity of phase make a complete set, thus allowing us to solve for the frequencies and wave numbers.

Reflected wave: $-k_i v_f=k_r v_f-\omega_r$, with Eq. (A9), gives

$$\omega_r=\frac{k_i v_f}{1-\beta}=k_i c\beta(1+\beta)\gamma^2, \tag{A13}$$

and

$$k_r=\frac{k_i\beta}{1-\beta}, \tag{A14}$$

Body mode 1: $-k_i v_f=-k_1 v_f-\omega_p$,

$$k_1=k_i-\frac{\omega_p}{\beta c}, \tag{A15}$$

Body mode 2: $-k_i v_f=-k_2 v_f+\omega_p$,

$$k_1=k_i+\frac{\omega_p}{\beta c}, \tag{A16}$$

Transmitted wave: $-k_i v_f=-k_t v_f-\omega_t$,

$$\omega_t=(k_i-k_t)v_f. \tag{A17}$$

Substituting Eq. (A10) for ω_t into Eq. (A17) gives

$$k_t=\beta^2\gamma^2 k_i(-1\pm\sqrt{1+\kappa_p^2}), \tag{A18}$$

where

$$-\kappa_p^2=\frac{(\omega_p^2+\omega_c^2-k_i^2v_f^2)}{\beta^4\gamma^2k_i^2c^2}.$$

The physical solution is the root which makes k_t positive, therefore we take the plus sign in Eq. (A18). The upshifted transmitted frequency is obtained by using the appropriate expression for k_t, and is given by

$$\omega_t=(k_i-k_t)v_f=[1-\gamma^2\beta^2(-1+\sqrt{1+\kappa_p^2})]k_i\beta c. \tag{A19}$$

If $\kappa_p^2\ll 1$, then the square root term can be expanded to give an approximate expression for ω_t

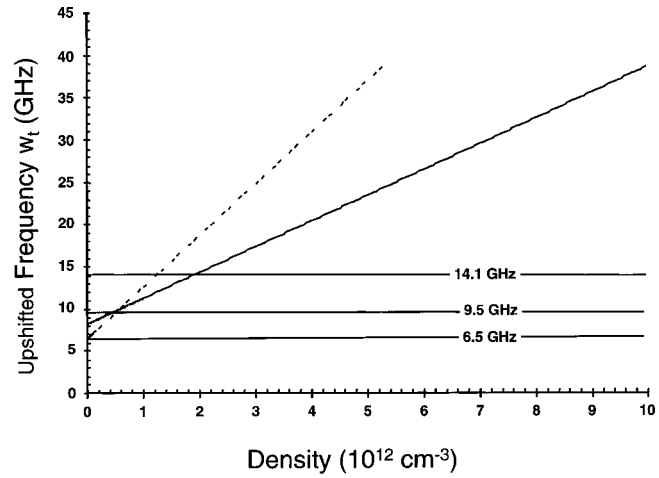

FIG. 13. Plot of the upshifted transmitted frequency as given by Eq. (A19) vs plasma density for two different pin spacings. The solid line is the result for the $d=1.1345$ cm, and the dashed line, for the $d=2.269$ cm case. Notice, that the further apart the pins are spaced, the higher the frequency upshift for a given plasma density. These results imply that for the same pressure different frequencies will be measured for the different pin spacings.

$$\omega_t\cong\left\{1-\gamma^2\beta^2\left[-1+\left(1+\frac{\kappa_p^2}{2}\right)\right]\right\}k_i\beta c,$$

$$\omega_t\cong\frac{k_i\beta c}{2}+\frac{(\omega_p^2+\omega_c^2)}{2\beta^2k_i^2c^2}. \tag{A20}$$

Evaluating the parameters of our experiment give the following value for κ_p^2, assuming a density of 10^{12} cm^{-3}

$$\beta=\sqrt{1-\frac{\omega_p^2}{\omega_l^2}}=1-10^{-10},$$

$$\gamma=\frac{1}{\sqrt{1-\beta^2}}=125\,313,$$

$$\omega_c=2\pi 6.5\ \text{GHz},$$

$$k_i=\frac{\pi}{2.269\ \text{cm}}=1.38\ \text{cm}^{-1}$$

gives

$$\kappa_p^2=1.16e-10.$$

With this value of κ_p, the approximation of Eq. (A20) is adequate for most cases. Equation (A19) is plotted in Fig. 13 for the two different pin spacings, d used in the experiment.

[1] D. Daniels, IEE Rev. **43**, 193 (1997).
[2] L. Carin, K. Agi, D. Kralj, K. M. Leung, and B. A. Garetz, IEEE J. Quantum Electron. **29**, 2141 (1993).
[3] B. I. Cohen, E. B. Hooper, T. B. Kaiser, E. A. Williams, and C. W. Dornier, *40th Annual Meeting of the DPP of the APS, New Orleans, LA*, May 1999 (American Institute of Physics, Woodbury, NY, 1999), Vol. 6, p. 1732.
[4] P. Muggli, R. Liou, J. Hoffman, T. Katsouleas, and C. Joshi, Appl. Phys. Lett. **72**, 19 (1998).
[5] C. H. Lai, R. Liou, T. C. Katsouleas, P. Muggli, R. Brogle, C. Joshi, and

Downloaded 14 Aug 2009 to 128.97.48.171. Redistribution subject to AIP license or copyright; see http://jap.aip.org/jap/copyright.jsp

W. B. Mori, Phys. Rev. Lett. **77**, 4764 (1996).
[6] W. B. Mori, T. Katsouleas, J. M. Dawson, and C. H. Lai, Phys. Rev. Lett. **74**, 542 (1995).
[7] Loading the waveguide with a periodic structure produces stopbands (see Fig. 5), but the experiment described here is run in a regime below the first stop band, thus the effect of the periodic structure on the fields is negligible for frequencies below 14 GHz, and reduces the field amplitude for frequencies close to 14.6 GHz.
[8] W. B. Mori, Phys. Rev. A **44**, 5118 (1991).
[9] Y. Nakato, T. Chiyoda, and H. Tsubomura, Chem. Soc. Jpn. Bull. **47**, 3001 (1974).
[10] J. R. Hoffman, P. Muggli, T. Katsouleas, W. B. Mori, and C. Joshi, ACC. Eighth Workshop Baltimore, MD, July 1998, p. 544.
[11] W. Shen, J. E. Scharer, N. T. Lam, B. G. Porter, and K. L. Kelly, J. Appl. Phys. **78**, 6974 (1995).
[12] For the cutoff waveguide at $\omega_c = 14.1$ GHz, a modification due to the stop band at 14.6 GHz of the step function profile was not used.
[13] M. Lampe, E. Ott, and J. H. Walker, Phys. Fluids **21**, 42 (1978).
[14] V. I. Semenova, Izv VUZ. Radiofizika **10**, 1077 (1967).

Downloaded 14 Aug 2009 to 128.97.48.171. Redistribution subject to AIP license or copyright; see http://jap.aip.org/jap/copyright.jsp